Electronic structure and phase stability study in the Ni-Ti system

A. Pasturel and C. Colinet
Expérimentation Numérique (DRED) et Physique Numérique des Systèmes Complexes (CNRS), Maison des Magistères, CNRS Boîte Postale 166, 38042 Grenoble, France

D. Nguyen Manh and A. T. Paxton
Department of Materials, University of Oxford, Parks Road, Oxford OX1 3PH, United Kingdom

M. van Schilfgaarde
SRI International, 333 Ravenswood Avenue, Menlo Park, California 94025
(Received 10 April 1995; revised manuscript received 13 July 1995)

We present the results of a phase stability study in the Ni-Ti system. In particular, the formation energies of the three $NiTi_2$, NiTi, and Ni_3Ti compounds have been calculated using the full potential linear-muffin-tin-orbital method. The correlation between the electronic concentration and the crystal structure is interpreted in terms of the filling of bonding states for the Ni_3Ti compound. Two sets of effective cluster interactions are determined allowing us to include bcc- and fcc-based solid solutions in the phase stability analysis. Ordering effects are treated by means of the cluster variation method. An attempt to calculate the composition-temperature phase diagram of the Ni-Ti system is proposed.

I. INTRODUCTION

Ni-Ti alloys do not only have properties that make them promising candidates for a new generation of high-performance alloys, but also exhibit phenomena which are of great interest for theoretical study. In particular, extensive research on the system has been stimulated by the unusual martensitic transformation[1] that has been found in alloys near equiatomic stoichiometry. This transformation is associated with the "shape memory" effect that has led to a variety of practical applications for these alloys.[2] Additional stimulation for the research has come from the finding that alloys on the Ti-rich side of the phase diagram, particularly through the composition range 60–70 at. % Ti, have glass-forming ability.[3] Moreover, near the stoichiometry $NiTi_2$, a metastable quasicrystal phase can be formed.[4]

Of primary importance in attempting to engineer the properties of the Ni-Ti alloys is an understanding of the equilibrium and metastable phases in the system and their range of (meta)stability with respect to experimentally controlled parameters such as composition and temperature. However, in spite of the extensive amount of research carried out so far on this system, thermodynamic research has been limited to a few investigations. An assessment of the experimental work which has been performed to study the equilibrium and metastable phases in this system can be found in Ref. 5, from which the phase diagram in Fig. 1 is redrawn. This assessed diagram is characterized by the occurrence of three intermediate phases: Ni_3Ti which melts congruently near 1653 K and whose structure is a hexagonal closed-packed superlattice,[6] NiTi which melts congruently near 1583 K and which has the CsCl-type structure[6] at elevated temperatures, and $NiTi_2$ which melts peritectically near 1257 K and which has a complex $E9_3$ cubic-type structure[6] with 96 atoms per unit cell. However, if there is no major disagreement concerning the extent of the single-phase NiTi region above 900 K, experimental observations have been a source of speculation and confusion on which path leads to the most stable state.[6] It is now accepted that the system undergoes a phase transition to the martensitic phase (B19′) involving several intermediate phases.[7,8] Another feature of great interest for theoretical study is the occurrence of metastable transition phases leading to the formation of the equilibrium Ni_3Ti $D0_{24}$ compound. Evidence for a metastable Ni_3Ti $L1_2$ phase has been found.[5]

Understanding of the microscopic origins of this type of structural selectivity has been at the core of structural chemistry, metallurgy, and condensed matter physics for a long time. Predictions of phase stabilities were often based on intuitive parameters such as electronegativities, electron concentration, atomic sizes, or orbital radii. Of particular interest to us here are the approaches that attempt to demystify structural selectivity directly in terms of the electronic structure. In this respect, recent advances in first-principles self-

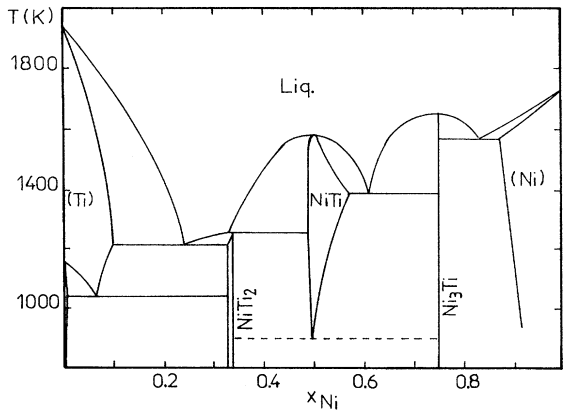

FIG. 1. Experimental phase diagram of the Ni-Ti system.

0163-1829/95/52(21)/15176(15)/$06.00

consistent formulations have produced a wealth of information on the ground-state properties of ordered intermetallic compounds. Given the crystal structure type of an ordered compound, one can calculate its equilibrium lattice parameters, elastic constants, phonon frequencies, and cohesive energy, often within a few percent of the measured values. To find the stable crystal configuration, one then repeats the total-energy calculation for a few other assumed crystal structures that by analogy with related compounds are expected to be likely competitors for the stable ground state. However, to get a complete phase diagram it is necessary to know the evolution of the structural stability as a function of the temperature.

The basic tools to study such an evolution, ordering and clustering phenomena, etc., are based on a generalized three-dimensional (3D) Ising model.[9] The problem consists then of two equally important parts, namely, (i) the quantum-mechanical determination of the 3D Ising model parameters, and (ii) the study of this model for $T>0$ K, using methods of statistical mechanics. The statistical part of the theory has already achieved a high level of sophistication. The traditional mean-field theory (Bragg-Williams approximation) is currently replaced by more advanced approaches. At present the most important ones seem to be the cluster variation method[10] (CVM) and Monte Carlo simulations.[11] In both approaches it is assumed that the configurationally dependent part of the internal energy can be written as a rapidly convergent sum of pair and multisite interatomic interactions.

The parameters entering the 3D Ising model are derived basically in two different ways. (i) A limited set of periodic crystal structures representative for a given problem is chosen and their total energies are calculated using first-principles self-consistent calculations. This method, proposed by Connolly and Williams,[12] was recently developed further by Zunger and co-workers[13] and is called the renormalized interaction approach. Standard *ab initio* band structure techniques applied to suitably chosen small supercells can be used and the double-counting terms are included. On the other hand, as the interaction energies, which are of order of a few mRy, are obtained as differences of total energies, the numerical requirements are severe. (ii) The multiple-scattering expansion of the thermodynamical potential for the statistically disordered alloy is the starting point for the generalized perturbation method (GPM) of Ducastelle and Gautier,[14] the concentration-waves theory (CWT) of Gyorffy and Stocks,[15] and the embedded-cluster method (ECM) of Gonis *et al.*[16] All these methods are based on the coherent-potential approximation (CPA) for the disordered state and quite recently they were employed in calculations of the Ising model parameters from first principles. Here the advantages are explicit expressions for the interatomic interaction parameters and thus physical transparency. The double-counting terms are neglected on the basis of the so-called force theorem,[17] but further efforts to clarify this point would be desirable.

In this paper we present preliminary results of an *ab initio* study of the c-T phase diagram in the Ni-Ti system. In such a study, the relative stability of the three occurring Ni_3Ti, NiTi, and $NiTi_2$ compounds have to be understood. Their formation energies are calculated using the linear-muffin-tin-orbital (LMTO) method[18,19] in order to analyze the microscopic origin of their stability at $T=0$ K. Two sets of effective cluster interactions (ECI's) are then derived for bcc- and fcc-based disordered alloy phases using the renormalized interaction approach. ECI's will be used in conjunction with the cluster variation method to determine many thermodynamic and structural properties as a function of composition and temperature for both (partially) ordered and disordered alloy phases. Furthermore, an attempt to calculate the Ni-Ti phase diagram will be presented.

The remainder of the paper is organized as follows. In Secs. II and III the details of the electronic structure calculations and the method of obtaining ECI's are presented and the microscopic origin of the stability of the compounds is discussed. In Sec. IV, a complete equilibrium phase diagram is calculated for the Ni-Ti system and compared with the experimental diagram.

II. TOTAL-ENERGY CALCULATIONS

As a first step, we have studied the relative structural stability of the three intermediate phases observed in the equilibrium phase diagram. In the structurbericht notation, these phases are called the hexagonal $D0_{24}$ (Ni_3Ti) phase, the cubic $B2$ (NiTi) high-temperature phase, the monoclinic $B19'$ (NiTi) low-temperature phase, and the cubic $E9_3$ ($NiTi_2$) phase.[6]

A. Computational details

To calculate the energies of these different phases described in Table I, we employ the all-electron total-energy local-density formalism as carried out with the linear-muffin-tin-orbital method and using two distinctly different approaches. In the first, the linear-muffin-tin orbitals are augmented with numerical solutions of the radial Schrödinger equation within nonoverlapping muffin-tin spheres. No spherical shape approximation for the potential or charge density is made; in the interstitial region, these quantities are expressed in Hankel-function expansions as proposed by Methfessel.[20] In the second approach, we employ the atomic-sphere approximation[19] (ASA) in which the spheres are permitted to overlap and are expanded until they fill the space. In addition, the so-called "combined correction term"[19] is included, which accounts for errors from overlapping the spheres and leaving regions not contained in any spheres due to the atomic-sphere approximation. For both approaches, the LMTO basis included s, p, and d functions for each atom. For the full-potential calculations, it is essential to extend the basis by using LMTO's with various localizations. In the present calculations we have used 22 augmented Hankel functions per Ni and Ti sites [s ($3K$'s), p ($3K$'s), d ($2K$'s)] where the corresponding decay energies are $-K^2=-0.01$ (spd), -1.0 (spd), and -2.3 Ry (sp). Accurate calculations of the bulk properties for these materials also require an extended treatment of the Ti and Ni $2p$ states. We have therefore included a second "semicore" panel to provide bandlike representation of both the Ti $2s$ and $2p$ states as well as the Ni $2s$ and $2p$ states, using the same Ni and Ti basis as for the upper panel, except for the appropriate reduction in the Ti and Ni s and p principal quantum numbers.[21] The local-density potential of von Barth and Hedin is used.[22] To evaluate integrals over the Brillouin zone,

TABLE I. Structure information of the three $MoPt_2$-, $MoSi_2$-, and $NiTi_2$-type structures.

Phase	System	Space group	Atoms/Cell	Lattice parameters (a.u.)	Atomic positions
$MoPt_2$	orthorhombic	$Immm$	6	$a=7.418$ $b=a/\sqrt{2}$ $c=3a/\sqrt{2}$	Mo $2(a)$ (0,0,0) Pt $4(g)$ (0,0,1/3)
$MoSi_2$	tetragonal	$I4/mmm$	6	$a=5.707$ $c=3.295a$	Mo $2(a)$ (0,0,0) Si $4(e)$ (0,0,1/3)
$NiTi_2$	cubic	$Fd\bar{3}$m	96	$a=21.398$	Ni $32(e)$ (x',x',x') Ti16(c) (1/8,1/8,1/8) Ti $48(f)$ $(x,0,0)$ $x'=0.912$ $x=0.311$

we use a uniform mesh of sampling points which ensure that the total energy is converged to within 0.1 mRy per atom. For the full-potential (FP) calculations, the charge density is calculated exactly in the muffin-tin spheres in angular momentum components up to $l=4$. We use the same angular momentum cutoff in the interpolation of quantities in the interstitial region, expanded in Hankel functions of energies -1 and -3 Ry.[21]

For each phase, the total energies provided by the LMTO method are obtained for different values of the volume; the minimum of this curve determines the equilibrium total energy and the equilibrium volume. The bulk modulus which is related to the curvature of the total energy with volume is obtained using a fit based on Murnaghan's equation of state.[23] Since the total energies for the pure metals are treated in the same way, the formation energy is obtained by subtracting the weighted sum of total energies of the constituent elements from the total energy of the compound, namely, $\Delta E=E_{\mathrm{Ni}_a\mathrm{Ti}_b}-(aE_{\mathrm{Ni}}^{\mathrm{fcc}}+bE_{\mathrm{Ti}}^{\mathrm{hcp}})$. It should be noted that the ground states of Ni and Ti are predicted to be fcc and hcp, respectively. The energy differences between the fcc, bcc, and hcp structures, defined as $\Delta E_{\mathrm{fcc\text{-}bcc}}=E_{\mathrm{coh}}^{\mathrm{fcc}}-E_{\mathrm{coh}}^{\mathrm{bcc}}$ and $\Delta E_{\mathrm{fcc\text{-}hcp}}=E_{\mathrm{coh}}^{\mathrm{fcc}}-E_{\mathrm{coh}}^{\mathrm{hcp}}$ are -3.9 and -2.9 kJ/mol and -1 and 5.5 kJ/mol for Ni and Ti, respectively. At high temperatures, the Ni-Ti phase diagram can be viewed as resulting from a bcc-fcc competition. Therefore it seems to be important to compare the stability of the three phases, namely, $D0_{24}$, $B2$, and $E9_3$ structures, with superstructures occurring on the fcc and bcc lattices.

B. Phase stability of $NiTi_2$ compound

The electronic structure and the relative structural stability of the $NiTi_2$ compound among the three different ($MoPt_2$-, $MoSi_2$-, and $NiTi_2$-type) structures have been already studied[24] and only the main conclusions are reported here. Among the topologically close-packed (tcp) phases, the $NiTi_2$-type structure displays a peculiar behavior since it is only partially tetrahedrally packed. It has 96 atoms per unit cell of the fcc Bravais lattice with three inequivalent site types (see Table I). Two of these sites (one Ti and one Ni) are icosahedrally coordinated while the remaining site has 14 neighbors. The stability of the $NiTi_2$-type structure has been studied versus $MoPt_2$-type and $MoSi_2$-type structures which can be viewed as being superstructures of the fcc lattice and the bcc lattice, respectively. In Table II, we present the formation energies of the $NiTi_2$ compound in the three candidate structures using self-consistent FP and ASA calculations. In agreement with experiment, the $NiTi_2$-type structure has the lowest formation energy among the three structures. The shape approximation made in the ASA is acceptable since ASA calculations give the same hierarchy as the FP ones. However, if the FP-calculated formation energy of the

TABLE II. Formation energies (in kJ/atom) for the $NiTi_2$ compound in the three structures. Comparison with experimental values.

	LMTO-ASA theory	FP-LMTO theory	Experimental values
$NiTi_2$ type	-33.7	-28.2	-26.8 (Ref. 53) -29.3 (Ref. 54)
$MoPt_2$ type	-18.7	-10.2	
$MoSi_2$ type	-31.1	-23.1	

TABLE III. Structure information of the four $L1_0$-, $B19$-, $B2$-, and $B19'$-type structures.

Phase	System	Space group	Atoms/Cell	Lattice parameters (a.u.)	Atomic positions
$B2$	cubic	$Pm\bar{3}m$	2	$a=5.69$	Ni 1(a) (0,0,0) Ti 1(b) (0.5,0.5,0.5)
$B19'$	monoclinic	$P2_1/m$	4	$a=5.452$ $b=8.734$ $c=7.786$ $\gamma=96.8$	Ni 2(a) (x,y,0.25) $x=0.0525$ $y=0.193$ Ti 4(e) (x',y',0.75) $x'=0.5247$ $y'=0.279$
$B19$	orthorhombic	$Pmma$	4	$a=8.90$ $b=5.45$ $c=9.44$	Ni 2(f) (0.25,0.5,x) $x=0.188$ Ti 2(e) (0.25,0, x') $x'=0.687$
$L1_0$	tetragonal	$P4/mmm$	4	$a=7.17$ $c=7.17$	Ni1 (1a) (0,0,0) Ni2 (1c) (0.5,0.5,0) Ti (2e) (0,0.5,0.5)

$NiTi_2$-type structure is in very good agreement with the experimental one, the ASA-calculated formation energy by 20% overestimates the experimental one.

C. Phase stability of NiTi compound

The shape-memory effect exhibited by NiTi alloys near equiatomic composition is related to a reversible martensitic transformation which occurs near room temperature. NiTi crystallizes at low temperature in a monoclinic structure ($B19'$ NiTi) while the high-temperature β phase has the simple cubic $B2$ structure. On cooling the $B2$ structure below the martensitic transformation temperature, the system undergoes a displacive structural transformation to an intermediate or so-called R phase and then undergoes a martensitic transformation to the monoclinic $B19'$ structure. Several mechanisms for the martensitic transformation of $B2$-phase alloys have been proposed.[25–28] One of the major factors determining the transformational behavior of these phases in the presence of anomalies in the phonon system; according to Zhao and Harmon,[29] the soft phonon which is responsible for the premartensitic phase transformation in $B2$-phase NiTi is found to arise from the strong electron-phonon coupling of nested electronic states on the Fermi surface. Thermal vibrations and changes in electronic occupation cause a smearing of the nested features which in turn cause a hardening of the phonon anomaly. As a first step of this very intricate study, we propose to study the structural stability of the NiTi compound at $T=0$ K. Indeed, the knowledge of the limiting values of the total energies for vanishing temperature and their volume dependence can provide useful information about the shape of the phase diagram near the transformation temperature. The relative structural stability of the NiTi compound is determined among four different structures, namely, the simple cubic $B2$ structure and the monoclinic $B19'$ structure but also the tetragonal $L1_0$ structure and the orthorhombic $B19$ structure (see Table III). The $L1_0$ structure can be viewed as being a superstructure of the fcc lattice and a large number of transition-metal compounds can be described from it. The orthorhombic $B19$ phase is the low-temperature structure obtained in the isoelectronic PdTi system; however, in this system, the martensitic phase transition occurs at higher temperature and without formation of intermediate phases. As a starting point, we have performed FP total-energy calculations for varying volumes in order to locate the equilibrium lattice constants. In agreement with experiment the $B19'$ monoclinic structure has the lowest total energy among the four studied structures but the $B2$ structure is lying only 2 kJ/atom higher. In comparison, the values obtained for $L1_0$ and $B19$ structures are much higher than the value obtained for the ground state (see Table IV). This close value shows that external effects like temperature effects can lead to the reversible $B19'$-$B2$ transformation. The calculated formation energy of the NiTi compound, $\Delta E = -36.0$ kJ/atom can be compared with the experimental one, $\Delta E = -33.9$ kJ/atom. To check the applicability of the ASA to this structural study, we have performed the same self-consistent calculations in this approximation. From Table IV we see that the ASA calculations give the same hierarchy as the FP ones. However, the ASA-calculated formation energies overestimate the FP ones by 15%.

TABLE IV. Formation energies (in kJ/atom) for the NiTi compound in the four structures. Comparison with experimental values.

	LMTO-ASA theory	FP-LMTO theory	Experimental values
$B2$ type	−38.1	−36.0	−33.9 (Ref. 55) −34 (Ref. 56)
$B19'$ type	−39.8	−37.8	
$B19$ type	−34.5	−29.2	
$L1_0$ type	−36.7	−31.3	

In order to understand the phase stability from the microscopic point of view, we inspect the density of states (DOS) of the NiTi compound in the four structures (Fig. 2). The total DOS shows a common overall feature for all the structures, namely, a bonding-antibonding behavior due to the hybridization between the Ni states and the Ti states. This covalent interaction is in fact a salient feature of the Ni-Ti system and is also observed for the $NiTi_2$ compound[24] and for the Ni_3Ti compound (see below). More particularly, the DOS's are very similar for both the $B2$ and $B19'$ structures while the difference from the DOS's obtained from the $L1_0$ and $B19$ structures is more pronounced. Because of the lower symmetry of the $B19'$ structure, which removes the degeneracy of bands, the DOS of the $B19'$ phase shows more structure and peaks of smaller intensity than found for the $B2$ structure. The DOS at the Fermi level is roughly 20% lower for the $B19'$ phase than for the cubic $B2$ phase. This is mainly due to the fact that mixing between Ti states and Ni states is reduced in the martensitic phase compared to the cubic phase. It should be noted that the DOS's of $B19'$ and $B2$ NiTi phases are very similar to the DOS published in Ref. 30.

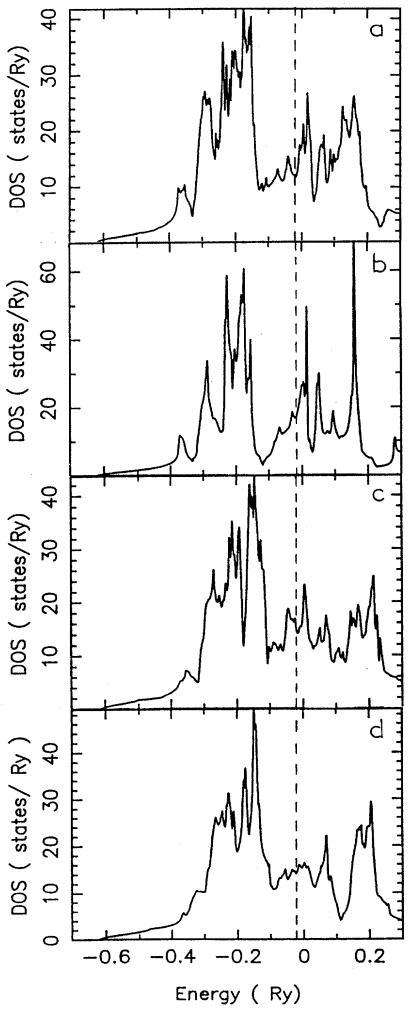

FIG. 2. Total densities of states for the NiTi compound in the four $B19'$ (a), $B2$ (b), $B19$ (c), and $L1_0$ (d) structures.

D. Phase stability of Ni_3Ti compound

The stoichiometric Ni_3Ti compound displays a four-layer, hcp, ordered structure, namely, the $D0_{24}$ structure. It has been shown that the precipitation of equilibrium Ni_3Ti from supersaturated solid solutions of Ni at low temperatures is preceded by a metastable phase called γ' with the $L1_2$ structure.[5] Therefore the study of the relative structural stability of the Ni_3Ti compound includes the $L1_2$, $D0_{24}$, and $D0_{22}$ structures (see Table V). The FP total energies are calculated for varying lattice constants in order to locate the equilibrium lattice constant and to determine the relative stability between phases (Table VI). The $D0_{24}$ structure has the lowest formation energy with the $L1_2$ phase lying only 0.5 kJ/atom higher. This appears to be consistent with the fact that the $L1_2$ phase is observed as the metastable γ' phase. The difference from the $D0_{22}$ structure is more pronounced but this difference is still small in comparison with the usual energy differences observed between the stable and unstable phases.[9] From Table VI it can be seen that the ASA calculations give the same hierarchy as the FP ones and the quantitative agreement between both approaches is correct. It should be noted that our results are in close agreement with the ones published in Ref. 31.

The total DOS's for the three $L1_2$, $D0_{22}$, and $D0_{24}$ structures are displayed in Fig. 3. As for $NiTi_2$ and NiTi compounds the overall shape of the DOS can be explained from a strong bonding interaction between Ni states and Ti states. For the three structures a deep valley or pseudogap separates the bonding and antibonding states; it can be shown that the Ni d character is found predominantly in the region below the pseudogap while the Ti d states are located mainly above the pseudogap. For the $L1_2$ structure, the Fermi level resides right on the peak in the antibonding region while for the $D0_{22}$ structure the Fermi level lies on the shoulder of a peak in the bonding region. On the other hand, the Fermi level for

TABLE V. Structure information of the three $D0_{22}$-, $L1_2$-, and $D0_{24}$-type structures.

Phase	System	Space group	Atoms/Cell	Lattice parameters (a.u.)	Atomic positions
$D0_{24}$	hexagonal	$P6_3/mmc$	16	$a=9.654$ $c=15.683$	Ni1 6(g) (0.5,0,0) Ni2 6(h) (x,2x,0.25) $x=-1/6$ Ti1 2(a) (0,0,0) Ti2 2(b) (x',2x',0.25) $x'=1/3$
$D0_{22}$	tetragonal	$I4/mmm$	8	$a=6.81$ $c=6.81$	Ni1 2(b) (0,0,0.5) Ni2 4(d) (0,0.5,0.25) Ti 2(a) (0,0,0)
$L1_2$	cubic	$Pm\bar{3}$m	4	$a=6.81$	Ni 3(c) (0,0.5,0.5) Ti 1(a) (0,0,0) Ti 48(f) (x,0,0) $x'=0.912$ $x=0.311$

the $D0_{24}$ structure is just located in the pseudogap. This implies that for the $D0_{24}$ structure the valence electrons are more efficiently packed in the bonding region, resulting in a stronger structural stability compared with the other structures. Based upon these arguments, we presume that the structural stability for the Ni_3Ti compound can be interpreted in terms of a band structure energy contribution to the total energy. To check such a qualitative discussion, we have used the force theorem and its application to ASA calculations.[32] In such an approach, the energy difference between two structures of the same composition $S1$ and $S2$ requires two steps. The first step is to obtain the self-consistent ASA potentials for structure $S1$, varying the atomic-sphere radii until the spheres are neutral. The second step consists of rearranging the atomic spheres so as to assemble the atoms in structure $S2$ and solve the Schrödinger equation once using the self-consistent potential parameters from structure $S1$. The total-energy difference between self-consistent $S1$ and structure $S2$ in the trial potential extracted from $S1$ is simply the difference in band structure energies for the two calculations.

In Table VII we illustrate the procedure for the Ni_3Ti compound with the $L1_2$ structure as the $S1$ structure and $D0_{22}$ and $D0_{24}$ structures as the $S2$ structure. We note that in comparison with self-consistent calculations the method is very successful. Within the same assumptions, it is also possible to interpret the structural trend as a function of the number of electrons per atom, e/a. By using the rigid-band approximation (RBA),[33] we have calculated the band structure energies of the $D0_{24}$ and $D0_{22}$ structures relative to $L1_2$ as a function of e/a; the resulting energy differences are shown in Fig. 4 where for each value of e/a the curve having the lowest energy indicated the predicted stable structure. The structural trend predicted by the RBA for A_3B transition-metal intermetallics goes from the $L1_2$ phase to the $D0_{24}$ phase and then to the $D0_{22}$ phase as a function of the number of electron per atom. In the low-e/a region, both the cubic $L1_2$ and the hexagonal $D0_{24}$ phases are more stable than the tetragonal $D0_{22}$ phase; for e/a above 8.58, the tetragonal $D0_{22}$ phase is the most stable phase. The stable hexagonal $D0_{24}$ phase emerges only in the e/a region be-

TABLE VI. Formation energies (in kJ/atom) for the Ni_3Ti compound in the three structures. Comparison with experimental values.

	LMTO-ASA theory	FP-LMTO theory	Experimental values
$D0_{24}$ type	−47.1	−47.6	−34.7 (Ref. 53) −42.9 (Ref. 54)
$D0_{22}$ type	−43.8	−42.9	
$L1_2$ type	−46.7	−47.1	

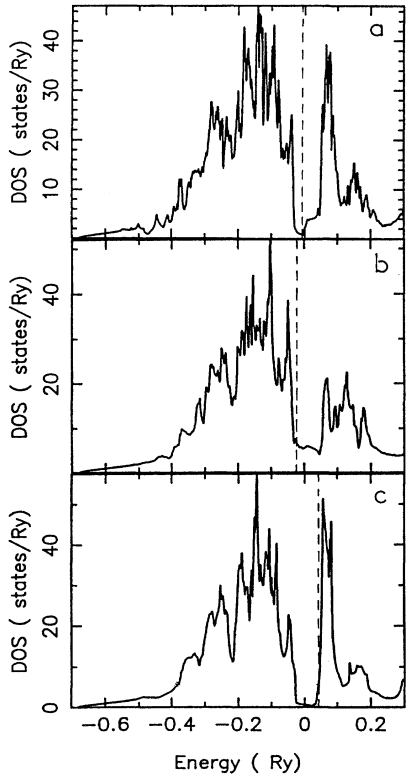

FIG. 3. Total densities of states for the Ni_3Ti compound in the three $D0_{24}$ (a), $D0_{22}$ (b), and $L1_2$ (c) structures.

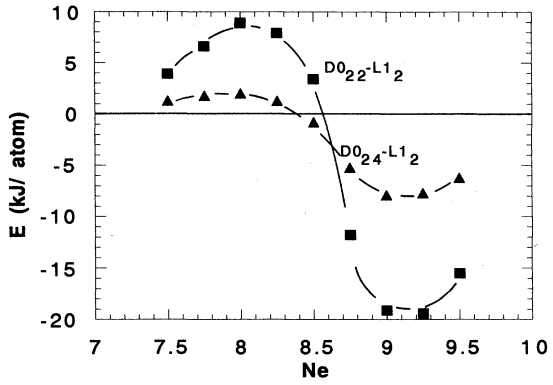

FIG. 4. Energy of $D0_{24}$ and $D0_{22}$ structures relative to $L1_2$ structure (in mRy/atom) as a function of the average valence-electron number per atom.

tween 8.41 and 8.58. Note that our results are in good agreement with experimental data[34] which show a strong correlation between e/a and crystal structure for the close-packed ordered A_3B transition-metal intermetallics. In particular, Sinha[35] showed that at $e/a=8.65$ the close-packed layers change from "triangular" T (related to the $L1_2$ structure) to "rectangular" R (related to the $D0_{22}$ structure). Thus our approach satisfies the statement that a simple RBA of the type described above can predict correctly the structural energy differences for at least some of the A_3B compounds of interest here.

III. CLUSTER EXPANSIONS AND EFFECTIVE CLUSTER INTERACTIONS

As discussed in the Introduction, the study of the evolution of the structural stability as a function of temperature requires one to define the parameters of the 3D Ising model. We use the renormalized interaction approach,[13] assuming that the total energy of an A_xB_{1-x} alloy can be described in terms of rapidly convergent series of concentration-independent multisite interactions. More precisely we assume that the total energy of a particular configuration α is expressed by

$$E^{\alpha}_{\rm tot}(r)=\sum_{\gamma}^{\gamma_{\max}} V_{\gamma}(r)\xi^{\alpha}_{\gamma}. \tag{1}$$

$V_\gamma(r)$ is the concentration-independent multisite interaction associated with the multisite correlation ξ^{α}_{γ} defined as

$$\xi_{\gamma}=\frac{1}{N_{\gamma}}\sum_{|n_j|}\sigma_{n_1}\sigma_{n_2}\cdots\sigma_{n_{\gamma}}, \tag{2}$$

where $\sigma_n=1-2p_n$ takes the value $+1$ or -1 depending on the occupancy of site n, N_γ is the total number of γ-type clusters, and the sum runs over all γ-type clusters that can be formed by combining sites on the entire crystal. From a finite number of total energies for ordered structures and by truncating the summation of (1), a set of multisite interactions is obtained from

$$V_{\gamma}(r)=\sum_{\alpha}(\xi^{\alpha}_{\gamma})^{-1}E^{\alpha}_{\rm tot}(r), \quad \phi<\gamma<\gamma_{\max}$$

$$V_{\gamma}(r)=0, \quad \gamma_{\max}<\gamma<\infty. \tag{3}$$

ϕ is the empty cluster. Since $E^{\alpha}_{\rm tot}(r)$ is generally a function of volume, the interactions $V_\gamma(r)$ depend on r too.

For instance, this set of structures is chosen in such a way as to determine the chemical interaction parameters for all clusters up to the regular nearest-neighbor tetrahedron cluster in the fcc lattice. Within this approximation we need only the values of the pure fcc metal energies and three values of

TABLE VII. Energy of $D0_{22}$ and $D0_{24}$ structures relative to $L1_2$ structure (in mRy/atom) for the Ni_3Ti compound. In column I, ASA self-consistent calculations, column II, FP self-consistent calculations, and column III, force theorem with the self-consistent potential parameters for the $L1_2$ structure.

$\Delta E(D0_{22}$-$L1_2)$			$\Delta E(D0_{24}$-$L1_2)$		
I	II	III	I	II	III
2.9	4.2	3.4	−0.4	−0.5	−0.8

ordered compound energies including NiTi in the $L1_0$ structure and Ni_3Ti and $NiTi_3$ in the $L1_2$ structure. In practice we have to judge the adequacy of this set by the extent to which the interaction parameters extracted from it are transferable to the description of other configurations; another way to check its convergence is to start from a rather large set of clusters and reduce their number on the basis of convergence tests. The ultimate question is to know if the geometry of the added clusters influences the convergence of the main interactions. For instance, many of the fcc phases which are observed in metallic systems can be stabilized by first- and second-neighbor pair interactions, and for this reason all clusters within this range have been included in this study. Furthermore, several studies[36] have shown that the third- and fourth-neighbor pair ECI's have to be included to obtain a good convergence of the expansion as written in (1). Additionally it has been shown that linear many-body cluster interactions are often sizable.[9] Therefore the set of ECI's will include also the linear triplet $E(3,4)$, the third- and fourth-neighbor pairs $E(2,3)$ and $E(2,4)$, and the triangles consisting of one second- (or third-) and two first-neighbor pairs, $E(3,2)$ and $E(3,3)$; the irregular tetrahedron $E(4,2)$ and the square of nearest neighbors $E(4,3)$ are considered as well in this study.

To perform such calculations, we have used a set of ordered compounds where the complementary structures are the $D0_{22}$ body-centered tetragonal structure for Ni_3Ti and $NiTi_3$ compounds, the $MoPt_2$ body-centered orthorhombic structure for Ni_2Ti and $NiTi_2$ compounds, and the body-centered tetragonal 40 phase and the $L1_1$ rhombohedral phase for NiTi compounds.[37] The strategy to obtain the optimum set of cluster interactions from the 11 structures considered in this paper is as follows.

For a given $\gamma_{\max}$ the best set of cluster interactions has been chosen as the one which minimizes the predictive error in the energy according to

$$\sum_{\alpha}^{11} \omega_{\alpha}\left[E^{\alpha}_{\rm tot}(r)-\sum_{\gamma}^{\gamma_{\max}} V_{\gamma}(r)\xi^{\alpha}_{\gamma}\right]^2 = \min \qquad (4)$$

with the weights $\omega_\alpha = 48N_c(\alpha)/N_G(\alpha)$; here $N_c(\alpha)$ and $N_G(\alpha)$ are the number of atoms per unit cell and the number of point group operations for the structure α, respectively. Formula (4) was suggested by Lu *et al.*[37] We find that different choices of weighting factors ω_α marginally affect the extracted ECI's.

The optimum set of ECI's is then obtained by studying the convergence of the predictive error involved in predicting energy values but also the convergence of the formation energy of the random alloy at 50 at. % Ti.[38] This latter one is also a significant check as it is obtained as a by-product in the used method.

The determination of an optimum set of ECI's in the bcc lattice follows the same idea; to perform such calculations, we have used a set of ordered compounds which includes the pure bcc metals, Ni_3Ti and $NiTi_3$ compounds in the cubic $D0_3$ structure, $NiTi_2$ and Ni_2Ti compounds in the body-centered tetragonal $MoSi_2$ structure, and the NiTi compound in the cubic $B2$ and $B32$ structures, in the tetragonal $B11$ structure, and in the orthorhombic $A1$ structure.[37]

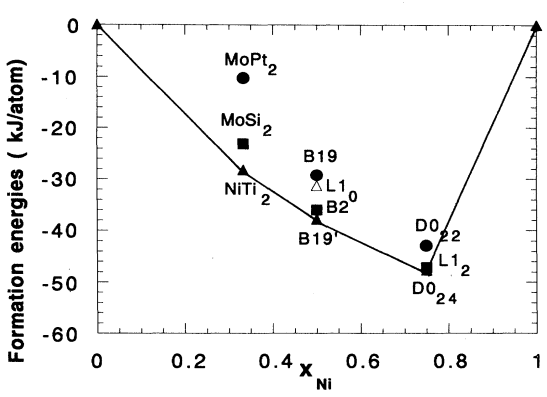

FIG. 5. Formation energies of Ni-Ti intermetallic compounds as calculated by the FP-LMTO method vs the atomic composition of Ti. The solid lines connect the energetically stable structures.

IV. PHASE DIAGRAM CALCULATIONS

A. Results of electronic structure calculations

The calculated values of the formation energies of the three compounds in the studied structures are plotted versus the composition in Fig. 5. Among the structures previously considered, the most energetically favorable intermetallic phases are the $D0_{24}$ Ni_3Ti, $B19'$ NiTi, and $E9_3$ $NiTi_2$ compounds in complete agreement with experimental features. The $L1_2$ and $D0_{22}$ structures are unstable at 25% Ti, while the $B2$, $B19$, and $L1_0$ structures are unstable at 50% Ti. As discussed previously, the difference in the calculated ΔE of the $B2$ and $B19'$ phases seems rather weak.

However, to explain the martensitic transformation occurring near room temperature, the entropy change must be consistent since the transformation temperature in this case is very low. Presumably vibrational entropy is the primary contribution to ΔS and we are still not prepared to estimate that. Therefore we shall present only the high-temperature part of the Ni-Ti phase diagram. There is great experimental controversy about the question of whether the eutectoid decomposition of NiTi to $NiTi_2+Ni_3Ti$ (at $T=903$ K) properly belongs to the equilibrium diagram. Our results locate the formation energy of the $B2$ structure just below the line drawn between the ΔE for the $D0_{24}$ structure and the $E9_3$ structure. However, results at $T=0$ K are not sufficient to give indications at high temperatures and again thermal effects have to be correctly included.

At 66% Ti, the $E9_3$ structure is the most stable one while the $MoSi_2$ and $MoPt_2$ structures are unstable with respect to the equilibrium NiTi ($B19'$)$\leftrightarrow$Ti(hcp). More generally the calculated formation energies of Fig. 5 are skewed in favor of Ni-rich compositions. The most stable compounds are found in the Ni-rich side of the phase diagram with a very stable $D0_{24}$ phase. As discussed previously in Sec. III, this is due to band-filling effects. For each studied structure, the Ni-like subbands lie below those of Ti and play the role of bonding states. Large ΔE is associated with having the lower-lying subbands (such as Ni's) filled and the higher-lying "antibonding" subbands (Ti's here) empty. This situation requires the occurrence of a well-defined pseudogap, separating the bonding states from the antibonding ones, and an electronic concentration in such a way that the Fermi

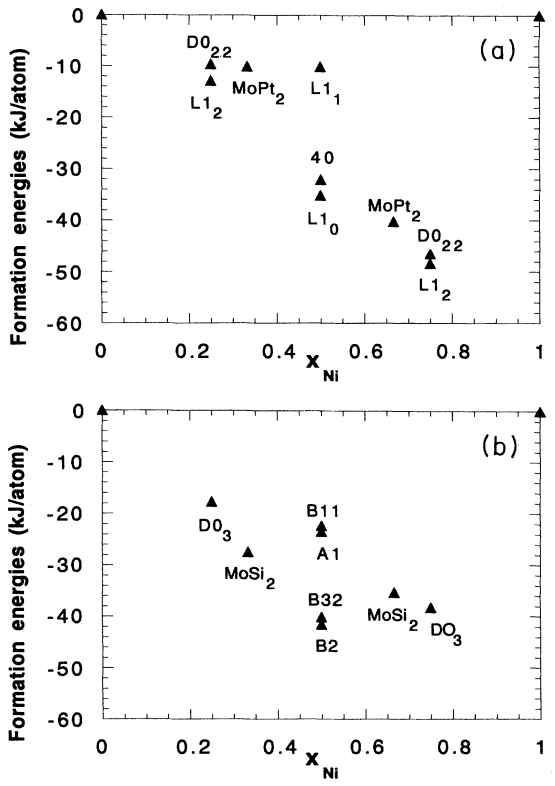

FIG. 6. Formation energies of fcc (a) and bcc (b) intermetallic compounds as calculated by the FP-LMTO method vs the atomic composition of Ti.

level is located in the pseudogap. This is the case for the $D0_{24}$ and $L1_2$ Ni_3Ti compounds which display a very well-defined pseudogap (see Fig. 3) while the pseudogap is much less pronounced for Ti-richer compounds (see Fig. 2 for instance). This asymmetry is the rule in the phase diagrams of alloy systems involving one member from the beginning and the other from the end of the transition-metal rows.

Another result to confirm this trend is to display the formation energies of the bcc and fcc superstructures used to calculate the ECI's. Only the non-spin-polarized values are presented since the ECI's will be used only to model the high-temperature part of the phase diagram. These values are displayed in Figs. 6(a) and 6(b). Both sets of values display the same asymmetrical shape. Superstructures with very high negative ΔE are found in the Ni-rich side, namely, $L1_2$ and $D0_{22}$ for the fcc lattice and $D0_3$ for the bcc one; for 75% Ti, the same structures are found unstable with respect to the equilibria NiTi ($L1_0$)↔Ti(fcc) and NiTi ($B2$)↔Ti(bcc), respectively. We shall see in the next section that this asymmetry can only be modeled by a set of ECI's which either are concentration dependent or include multiatom (i.e., more than two atoms) interactions. The consequences for the coherent phase diagrams will also be discussed.

B. Effective cluster interactions

1. fcc lattice

We have determined the optimum sets of ECI's in the fcc lattice containing between six and nine of the interactions corresponding to the clusters described in Sec. III. Since the energy curve for fcc Ni-Ti alloys is highly asymmetric around $x=0.5$, it is expected that multiatom interactions have to be included in the cluster expansion in order to reproduce it. For a given number of interactions, the set of ECI's is selected after considering a hierarchy of fits to the *ab initio* results of 11 structures. For the set of six interactions, the total energies of ordered structures are reproduced with a root-mean-square error of 1 mRy/atom while this error becomes smaller than 0.2 mRy/atom for the set of nine interactions. For the set of six interactions, the data of Table VIII show that the optimum set consists of the empty and point clusters, the nearest- and next-nearest-neighbor pairs, $E(2,1)$

TABLE VIII. The effective cluster interactions for fcc-based Ni-Ti alloys.

Symbol coordinates	Multiplicity	6D set	7D set	8D set	9D set
$E(0,1)$	1	−19.64	−19.64	−18.37	−19.00
$E(1,1)$ (000)	1	−18.91	−23.64	−23.64	−23.64
$E(2,1)$ (000), (1/2 0 1/2)	6	27.84	27.84	31.14	29.74
$E(2,2)$ (000), (100)	3	−9.70	−9.70	−10.05	−10.07
$E(2,3)$ (000), (1 1/2 1/2)	24			−4.53	−3.12
$E(2,4)$ (000), (101)	6				0.65
$E(2,5)$ (000), (3/2 0 1/2)	6				
$E(3,1)$ (000), (1/2 1/2 0), (1/2 0 1/2)	8	18.91	17.27	17.27	17.27
$E(3,2)$ (000), (1/2 0 1/2), (100)	12		6.37	6.37	6.37
$E(3,3)$ (000), (1/2 0 1/2), (1 1/2 1/2)	24				
$E(3,4)$ (000), (1/2 0 1/2), (101)	6				
$E(4,1)$ (000), (1/2 0 1/2), (1/2 1/2 0) (0 1/2 1/2)	2	1.50	1.50	1.81	1.81
$E(4,2)$ (000), (1/2 0 1/2), (1/2 1/2 0) (100)	12				
$E(4,3)$ (1/2 0 1/2), (0 1/2 1/2), (1/2 1 1/2), (1 1/2 1/2)	3				

TABLE IX. *Ab initio* calculated values and predicted values for both Ni_4Ti and $NiTi_4$ compounds.

Compounds	FP LMTO	6D set	7D set	8D set	9D set
$NiTi_4$	−8.5	−11.94	−9.20	−9.73	−9.86
Ni_4Ti	−35.3	−34.64	−36.72	−37.25	−37.38

and $E(2,2)$, the nearest-neighbor isoceles triangle $E(3,1)$, and the nearest-neighbor regular tetrahedron $E(4,1)$. We find that, except for the empty and point clusters, the two largest ECI's are those for the nearest-neighbor pair interaction and the nearest-neighbor isoceles triangle. As expected, the large positive nearest-neighbor pair interaction suggests strong ordering tendencies which are enhanced in the Ni-rich alloys by the substantial value of the triplet $E(3,1)$ value. The data obtained for larger sets (up to nine interactions) confirm this first analysis. The third- and fourth-neighbor pair interactions are not found to be important in describing the total energy of the alloys in the Ni-Ti system. Similarly, the ECI's corresponding to quadruplets are found to be small, which suggests that the cluster expansion is already well converged with the interactions used. In order to test this convergence we have also compared the formation energies of the Ni_4Ti and $NiTi_4$ compounds (in the $MoNi_4$ tetragonal structure) determined by the cluster expansion with the formation energies determined by a direct calculation. Table IX shows that the agreement between both sets of data is correct even for the smallest set of ECI's.

The ECI's can be used to perform a complete ground-state search to find the structures which are energetically stable at $T=0$ K out of all possible configurations. Such a study has been undertaken by Lu and co-workers[39] and Wolverton *et al.*[40] for other metallic alloys systems. Here this study is of minor importance since no fcc superstructure is found to be a ground state in the Ni-Ti system. Instead we check the relative structural stability of the Ni_3Ti compound as calculated by the cluster expansion since we have found a very small difference between the $D0_{24}$ and $L1_2$ structures from direct calculations. For each set of ECI's, the formation energy of the $L1_2$ structure as calculated from the cluster expansion is found slightly more positive than the LMTO value (around 0.5 kJ/atom); then this value is always slightly more positive than the value of the $D0_{24}$ structure. Another interesting point is to check the stability of the Ni_8Ti compound since this phase occurs in the isoelectronic Pt-Ni system. The fact that this phase lies 2 kJ/atom above the line drawn between the ΔE for the $L1_2$ structure and the zero for pure Ni indicates that Ni_8Ti is calculated to be unstable with respect to a two-phase mix of Ni_3Ti ($L1_2$ structure) and pure Ni.

In the Ti-rich side, all the calculated formation energies of the studied fcc-based compounds are located above the line drawn between the ΔE for the $L1_0$ structure and the zero for pure Ti in its fcc metastable state. This indicates that no intermediate fcc phases are stable in this region of the phase diagram and again this is due to the large value of the triplet $E(3,1)$.

2. bcc lattice

For the bcc lattice, we find that a set of six interactions gives a predictive error in the energy less than 1 mRy/atom. This set consists of the empty and point clusters, the nearest- and next-nearest-neighbor pairs, the nearest-neighbor and next-nearest-neighbor isoceles triangle, and the nearest-neighbor and next-nearest-neighbor irregular tetrahedron. Except for the empty and point clusters, the two largest ECI's are those for the nearest-neighbor pair and the isoceles triangle (see Table X). As seen in Table X, the convergence of the cluster expansion is still very rapid and does not depend on the parent lattice, namely, bcc or fcc lattice. The asymmetry around $x=0.5$ is well pronounced (but less than in the fcc lattice) as indicated by the value of the triplet interaction. Note also that the next-nearest-neighbor pair interaction has not the same sign in both fcc and bcc lattices.

TABLE X. The effective cluster interactions for bcc-based Ni-Ti alloys.

Symbol coordinates	Multiplicity	6D set	7D set	8D set
$E(0,1)$	1	−27.62	−25.90	−25.43
$E(1,1)$ (000)	1	−9.97	−9.97	−9.97
$E(2,1)$ (000), (1/2 1/2 1/2)	4	21.06	21.82	21.14
$E(2,2)$ (000), (100)	3	8.47	8.51	6.95
$E(2,3)$ (000), (101)	6		−3.23	−3.85
$E(2,4)$ (000), (3/2 1/2 1/2)	12			2.52
$E(2,5)$ (000), (111)	4			
$E(3,1)$ (000), (1/2 1/2 1/2), (100)	12	9.97	9.97	9.97
$E(3,2)$ (000), (1/2 1/2 1/2), (101)	12			
$E(3,3)$ (000), (1/2 1/2 1/2), (111)	4			
$E(4,1)$ (000), (1/2 1/2 1/2), (1/2 1/2 −1/2), (100)	6	−1.91	−1.19	−1.34
$E(4,2)$ (000), (1/2 1/2 1/2), (1/2 1/2 −1/2), (110)	6			

These results are also confirmed by the calculations of the effective pair interactions obtained via the generalized perturbation method applied to the tight-binding formulation of the coherent-potential approximation (TB-CPA). Indeed these effective pair interactions are strongly concentration dependent and rapidly convergent since taking into account first- and second-nearest-neighbor interactions is sufficient to simulate the thermodynamic data of the Ni-Ti system.[41,42] Such a fast convergence is also found in the Ni-Al system.[43]

C. Phase equilibrium

If vibrational effects and electronic excitations are not taken into account, the expansion of the formation energy of the alloy A_xB_{1-x} as developed in Sec. III can be used in conjunction with the CVM expressions for the configurational entropy of an Ising lattice to form an approximate free-energy functional for the real alloy.

For the alloy in phase α, the Helmhotz free energy may be written

$$F=F^{\text{lin}}+E_f^{\alpha}-TS_f^{\alpha} \tag{5}$$

with $F^{\text{lin}}=xF_A+(1-x)F_B$. x is the composition of the A element, F_I the free energy of pure element I, and E_f^{α} and S_f^{α} are respectively the energy and entropy of alloy formation.

The first simplifying assumption regarding the evaluation of the total free energy is to assume that the free energy for the pure elements can be written as[43]

$$F_I=E_I^{\text{coh}}-TS_I^{\text{vib}} \tag{6}$$

in which the cohesive energy and the vibrational entropy are both temperature independent.

The second assumption is that S_f^{α} is a purely configurational term given by its CVM expression:

$$S_f^{\alpha}=\sum_{\gamma}\ \eta_{\gamma}\sum_{\sigma_{\gamma}}\ x_{\gamma}(\sigma_{\gamma})\ln x_{\gamma}(\sigma_{\gamma}). \tag{7}$$

In the present study, the tetrahedron approximation of the CVM has been used; the influence of other approximations on the shape of the Ni-Ti phase diagram will be discussed elsewhere.[44] The first sum of (7) is over all subclusters of the tetrahedron and the second sum is over the possible configurations on these subclusters. The η_{γ} are the Kikuchi-Baker coefficients[10,45] and $x_{\gamma}(\sigma_{\gamma})$ are referred to as cluster probabilities and are the ensemble averages of the fraction of clusters γ on the lattice which have the configuration σ_{γ}. These cluster probabilities are linearly related to the correlation functions.

As we have shown in Sec. III, it is necessary to include the second-neighbor pair interaction which is not a subcluster of the regular tetrahedron in the fcc lattice. For this cluster outside the range of the tetrahedron, the value of the correlation function at a given temperature and composition is obtained within the mean-field approximation.[44] The CVM expressions of the configurational entropy of the fcc and bcc lattices in the tetrahedron approximation can be found in Ref. 43.

In order to determine the equilibrium phase diagram, it is more convenient to minimize the grand potential Ω given by

$$\Omega=F-\mu\xi_1, \tag{8}$$

where μ is the effective chemical potential and ξ_1 the correlation function of the point cluster. The minimization is done using the natural iteration (NI) method developed by Kikuchi.[46] The NI equations used in the present model have been presented elsewhere[47] and will not be repeated here. The equilibrium phase diagram between the phases I and II is computed using the same scheme as proposed by Kikuchi and Murray.[48] For the same initial value of the effective chemical potential μ, the grand potentials of phases I (Ω_{I}) and II(Ω_{II}) are calculated according to (8). If $\Omega_{\text{I}}=\Omega_{\text{II}}$ the equilibrium conditions are realized, but if not, the value of μ is modified until $\Omega_{\text{I}}=\Omega_{\text{II}}$.

D. Phase diagram calculations

1. Thermodynamic analysis

Let us sum up the strategy of our calculations.

(i) The energies of the three compounds occurring in the phase diagram are obtained as a function of the volume. The minima of these curves are chosen to obtain the formation energies of these compounds. The entropies are considered to be equal to zero for the strictly stoichiometric compounds such as the Ni_3Ti compound but also for the $NiTi_2$ compound. For the NiTi $B2$ phase, the entropy of configuration will be given by the tetrahedron approximation of the CVM for ordered phases based on the bcc lattice.

(ii) The two solid solutions based on the fcc and bcc lattices are described as short-range-order solutions using the CVM treatment in its tetrahedron approximation. Computation of a coherent phase diagram, that is, a phase diagram composed of phases which are based on one lattice only, requires knowledge of $E_f^{\alpha}-TS_f^{\alpha}$ only, F_{lin} being a linear function of the composition. Thus the free energy of mixing is computed with the CVM. The incoherent Ni-Ti phase diagram requires $F_{\text{lin}}^{\text{fcc}}$ and $F_{\text{lin}}^{\text{bcc}}$ as well, or rather it requires the differences of these two linear terms, $\Delta F_{\text{lin}}^{\text{fcc-bcc}}=F_{\text{lin}}^{\text{fcc}}-F_{\text{lin}}^{\text{bcc}}$. The energy difference $\Delta E_{\text{coh}}^{\text{fcc-bcc}}$ is taken from FP-LMTO results at $T=0$ K. The theories concerning vibrational entropy require a detailed knowledge of elastic constants[49,50] and for the Ni-Ti system they must be able to model the martensitic transformation among other things. Such a study is beyond the scope of this paper and we shall present only the high-temperature part of the phase diagram. Therefore we use a simple empirical scheme for the vibrational entropy, namely, that the difference in the vibrational entropy between fcc and bcc lattices is a linear function of alloy composition and is independent of temperature. The vibrational entropy differences $\Delta S_{\text{vib}}^{\text{fcc-bcc}}$ for both elemental Ni and Ti are obtained from thermodynamic compilations.[51] In the same way, for the Ti hcp-bcc transformation, the vibrational entropy difference is computed from the cohesive energy difference of hcp and bcc allotropes at 0 K and from the experimental observation that the transition occurs at 1175 K.

(iii) The liquid phase is also described as a short-range-order phase using the tetrahedron approximation of the CVM free energy in the disordered fcc structure. The effective pair interactions are obtained from Carlsson's resummation procedure[52] which corresponds to a high-temperature expansion of the correlation functions. Although this model is de-

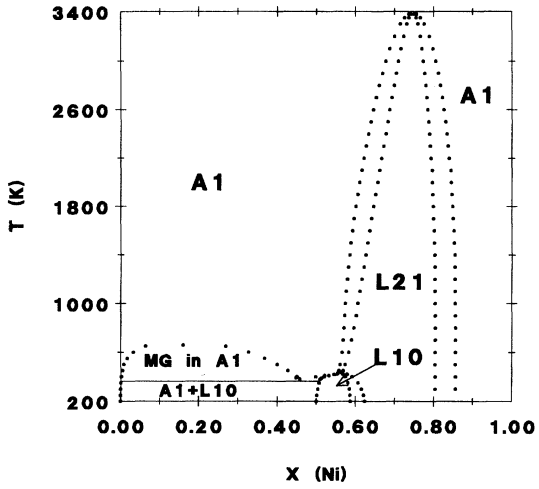

FIG. 7. The fcc coherent Ni-Ti phase diagram.

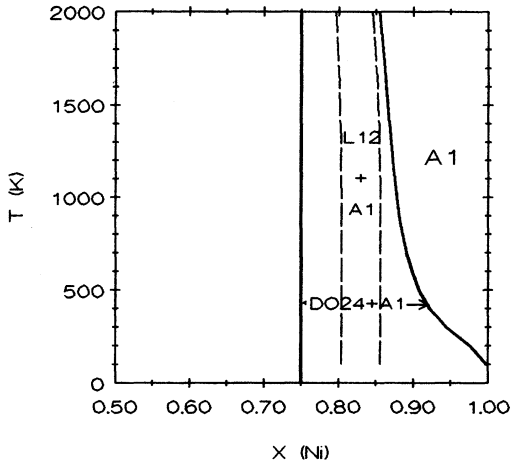

FIG. 8. Stable equilibrium Ni $(A1)\leftrightarrow Ni_3Ti$ $(D0_{24})$ and metastable equilibrium Ni $(A1)\leftrightarrow Ni_3Ti$ $(L1_2)$.

veloped with a solid-state approximation, it does a good job of describing the influence of chemical short-range order on the thermodynamic properties of the liquids.[43] Of course, the continuous phase space of the nuclei's motion and structural information, such as pair correlation functions, are lost. However, the chemical ordering contribution to the entropy and the energy, which are quantities of central interest in our calculations, are only proportional to the concentration fluctuations. Using a statistical approach based on a "discretized mesh" rather than the continuous phase of the nuclei's motion may be considered as correct to describe the concentration fluctuations.

However, there is still a "missing link" in our approach, which is the thermodynamic properties of the pure metals or, in other terms, the difference in free energy between the liquid and crystalline phases. Although the density-functional theory has made significant progress in the modeling of liquids, application to the determination of the melting temperature does not yet appear possible. Therefore we have chosen to use thermodynamic compilations to obtain melting temperatures $T_{\mathrm{Ni}}^{\mathrm{fcc\text{-}liq}}$ and $T_{\mathrm{Ti}}^{\mathrm{bcc\text{-}liq}}$ and the latent heats of melting $\Delta E_{\mathrm{Ni}}^{\mathrm{fcc\text{-}liq}}$ and $\Delta E_{\mathrm{Ti}}^{\mathrm{bcc\text{-}liq}}$ for both Ni and Ti elements.[51] In this case the free energy of these elements in their liquid state is given by

$$F_I^{\mathrm{liq}}(T)=E_I^{\mathrm{lat}}+\Delta E_I^{\mathrm{lat}\rightarrow\mathrm{liq}}-T(\Delta E_I^{\mathrm{lat}\rightarrow\mathrm{liq}})/(T_I^{\mathrm{lat}\rightarrow\mathrm{liq}}). \quad (9)$$

2. Phase diagrams

A schematic fcc Ni-Ti phase diagram can be obtained by comparing only the free energies of fcc and fcc-based superstructures like $L1_2$ and $L1_0$ structures. Figure 7 shows that the main features of this diagram are a miscibility gap (MG) with a maximum temperature of 660 K and two ordered phases $L1_2$ and $L1_0$ with transition temperatures of 3350 and 425 K, respectively. It should be noted that $L1_0$ displays a peritectoid decomposition leading to $L1_2$ and $A1$ phases above 425 K. As for the Ni-Al system,[42] the MG is caused by an elastic instability and can be understood through the concentration dependence of the calculated energy of mixing for the completely random fcc solid solution. A monotectoid decomposition between $L1_0$ and $A1$ phases at two different compositions occurs at 375 K. The $L1_2$ phase on the Ni-rich part displays a very stable phase behavior even if it does not occur in the equilibrium Ni-Ti phase diagram. In fact, as discussed in the Introduction, the $L1_2$ phase has been found as being a metastable phase and it is then interesting to compare the metastable equilibrium Ni $(A1)\leftrightarrow Ni_3Ti(L1_2)$ with the stable equilibrium Ni $(A1)\leftrightarrow Ni_3$ $Ti(D0_{24})$. The corresponding phase diagrams are shown in Fig. 8. It can be seen that, for temperatures above 1000 K and for a concentration range $0.75<x_{\mathrm{Ni}}<1$, the concentrations of the $A1$ phase are similar in the two equilibria, the $A1$ phase in the Ni $(A1)\leftrightarrow Ni_3Ti$ $(D0_{24})$ equilibrium being slightly more Ni rich than the $A1$ phase of the other equilibrium. In Fig. 9 are displayed the free-energy curves of the three $A1$, $L1_2$, and $D0_{24}$ phases as a function of x_{Ni} for $T=1500$ K. The conclusion is that it seems to be possible to obtain the metastable $L1_2$ phase from the $A1$ phase if rapid cooling is used, for instance.

Figure 10 shows the phase equilibria between bcc and bcc-based superstructures including $D0_3$ and $B2$ structures. The diagram exhibits a very stable $D0_3$ phase with a disor-

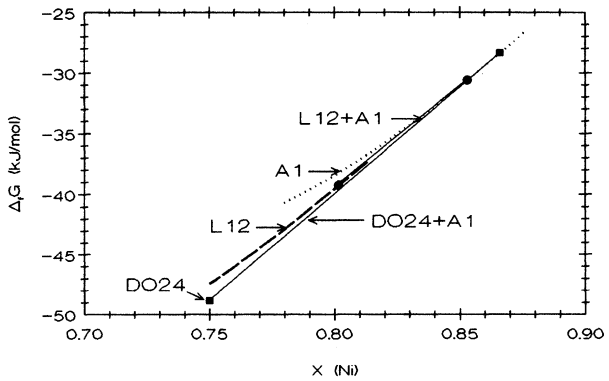

FIG. 9. Free-energy curves of $A1$ $(\cdots)$, $L1_2$ $(- - -)$, and $D0_{24}$ (—) phases at $T=1500$ K. ■—■ $A1\leftrightarrow D0_{24}$ equilibrium; ●—● $A1\leftrightarrow L1_2$ equilibrium.

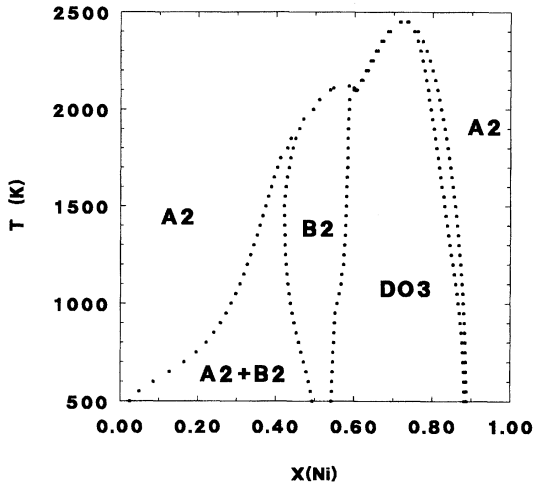

FIG. 10. The bcc coherent Ni-Ti phase diagram.

dering transition temperature of 2460 K, a pronounced NiTi $B2$ phase which is the high-temperature phase of the equilibrium phase diagram, and a metastable MG between $B2$ and $A2$ phases for Ti-rich alloys.

Let us emphasize the similarity of the two fcc and bcc phase diagrams. It is due to the similar behavior of formation energies of both bcc and fcc superstructures as a function of the composition. In the Ni-Ti system, the chemical interactions between Ni and Ti are so strong (see the value of the nearest-neighbor pair interaction) than they screen the underlying topology.

When both fcc- and bcc-based free-energy curves are combined with the liquid free energy and with the free energies of the three compounds, the complete phase diagram in Fig. 11 is obtained. We present only results concerning the high-temperature part of the phase diagram; this means that we do not include the martensitic transformation of the high-temperature $B2$ phase in the present calculations. At high temperatures, the Ni-Ti phase diagram can be viewed as resulting from a bcc-fcc competition. fcc dominates on the Ni side with the fcc solid solution and the metastable $L1_2$ (Ni_3Ti) phase which can precipitate from oversaturated solid solutions. On the Ti side, bcc dominates with an important bcc Ti terminal phase above 710 K. In the Ni-rich part, the agreement with the experimental phase diagram is good. The

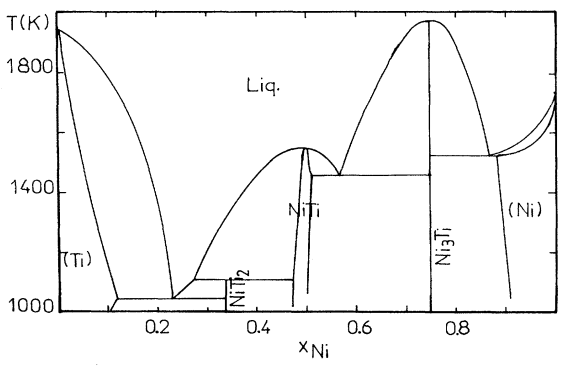

FIG. 11. The calculated Ni-Ti phase diagram.

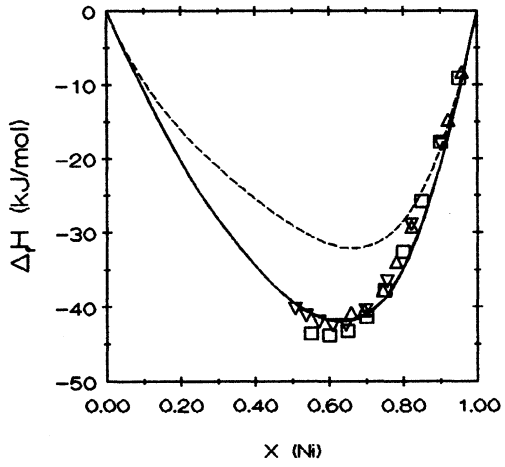

FIG. 12. Internal energies for the liquid phase ($T=2000$ K). Comparison between calculated (— with CSRO; --- without CSRO) and experimental values (□ Ref. 54; ▽ Ref. 53 at 1741 K; △ Ref. 53 at 1838 K).

congruently melting temperatures of Ni_3Ti and NiTi compounds are correctly predicted, like the eutectic temperature. More particularly, the Ni_3Ti compound is found to melt congruently at $T=1960$ K, 300 K above the experimental temperature. This overestimate of the melting temperature seems to be attributable to the overestimate of the formation energy of the Ni_3Ti compound. It should be noted that thermal effects on the energy and entropy of the studied compounds have not been taken into account in the calculations and that there is no alloy parameter to describe both the solid alloy part and the liquid alloy curve. For the liquid phase, it seems to be important to know if the approximations done to calculate the thermodynamic data are correct or not. Therefore we present calculations of internal energies at $T=2000$ K and compare our values to the experimental ones;[53,54] two sets of results are presented, one for completely disordered alloys, the other one for the equilibrium values of chemical short-range order (CSRO). From Fig. 12 it can be seen that the set of calculations which takes into account CSRO gives a very good description of the thermodynamic data of the liquid phase. Ordering effects are maximum around $x_{Ni}=0.7$ which is consistent with the occurrence of stable phases, namely, Ni_3Ti $L1_2$ and Ni_3Ti $D0_3$ phases in the fcc and bcc phase diagrams, respectively. In the liquid phase, the same effects, though reduced, are observed. On the Ti-rich part, the agreement is still very satisfying. The eutectic equilibrium is found to be between the $NiTi_2$ compound and the $A2$ terminal solution in agreement with experimental data and the most recent tight-binding calculations.[42] The calculated eutectic temperature is only 5 K higher than the experimental one.

V. CONCLUSION

It was shown that *ab initio* calculations are able to explain the stability of the different phases occurring in the Ni-Ti system. The high-temperature part of the Ni-Ti phase diagram has been obtained by combining total-energy LMTO calculations with the tetrahedron CVM approximation. No

vibrational effects have been taken into account. Only short-range order on fcc and bcc lattices has been introduced using CVM treatment in competition with the occurrence of complex phases like the $D0_{24}$ and $E9_3$ phases. The thermodynamic description of the liquid phase has been achieved by approximating this phase to a fcc-based disordered phase to minimize the number of parameters. The melting temperature and latent heat of the pure components are the only two parameters which have been introduced from outside the first-principles matrix. The results presented here are in many points in good agreement with the experimental data at high temperatures. We are therefore encouraged to continue this study by considering a more sophisticated thermodynamic description including thermal effects. The approach developed by Garbulsky and Ceder seems to be very promising to include such effects,[57] even if it requires the determination of the force constants for a three-dimensional alloy on an arbitrary lattice, which represents a formidable task for first-principles electronic structure methods.

ACKNOWLEDGMENTS

This work was supported by a computer grant at the Institut du Développement et des Ressources en Informatique Scientifique (IDRIS-CNRS).

[1] Z. Nishiyama, in *Martensitic Transformation*, edited by M. E. Fine, M. Meshii, and C. M. Wayman (Academic, New York, 1978).

[2] *Shape Memory Effects in Alloys*, edited by J. Perkins (Plenum, New York, 1975).

[3] T. Fukunaga, W. Watanabe, and K. Suzuki, J. Non-Cryst. Solids **61&62**, 343 (1984).

[4] C. Dong, Z. K. Hei, L. B. Wang, Q. H. Song, Y. K. Wu, and K. H. Kuo, Scr. Metall. **20**, 1155 (1986).

[5] *Binary Alloy Phase Diagrams*, 2nd ed., edited by T. B. Massalski (American Society for Metals, Metals Park, OH, 1990).

[6] *Pearson's Handbook of Crystallographic Data for Intermetallic Phases*, 2nd ed., edited by P. Villars and L. D. Calvert (American Society for Metals, Metals Park, OH, 1991).

[7] G. Herget, M. Müllner, J. B. Suck, R. Schmidt, and W. Wipf, Europhys. Lett. **10**, 49 (1989).

[8] X. Zhao, X. Wu, and T. Ko, Acta Metall. **37**, 1783 (1989).

[9] F. Ducastelle, *Order and Phase Stability, Cohesion and Structure*, edited by F. R. de Boer and D. G. Pettifor (North-Holland, Amsterdam, 1991), Vol. 3.

[10] R. Kikuchi, Phys. Rev. **81**, 988 (1951).

[11] K. Binder, in *Monte Carlo Methods in Statistical Physics*, edited by K. Binder, Topics in Current Physics Vol. 7 (Springer, Berlin, 1986).

[12] J. W. Connolly and A. R. Williams, Phys. Rev. B **27**, 5169 (1983).

[13] S. H. Wei, L. G. Ferreira, and A. Zunger, Phys. Rev. B **41**, 8240 (1990); Z. W. Lu, S. H. Wei, and A. Zunger, Phys. Rev. Lett. **66**, 1753 (1991).

[14] F. Ducastelle and F. Gautier, J. Phys. F **6**, 2039 (1976).

[15] L. Gyorffy and G. M. Stocks, Phys. Rev. Lett. **50**, 374 (1983).

[16] A. Gonis, X. G. Zhang, A. J. Freeman, P. Turchi, G. M. Stocks, and D. M. Nicholson, Phys. Rev. B **36**, 4630 (1987).

[17] A. R. Mackintosh and O. K. Andersen, in *Electrons at the Fermi Surface*, edited by M. Springford (Cambridge University Press, Cambridge, England, 1980).

[18] O. K. Andersen, Phys. Rev. B **12**, 3060 (1975).

[19] O. K. Andersen, in *Electronic Structure of Complex Systems*, edited by P. Phariseau and W. M. Temmerman (Plenum, New York, 1984), p. 11.

[20] M. Methfessel, Phys. Rev. B **38**, 1537 (1988).

[21] A. T. Paxton, M. Methfessel, and H. M. Polatoglou, Phys. Rev. B **41**, 8127 (1990).

[22] U. von Barth and L. Hedin, J. Phys. C **5**, 1629 (1972).

[23] F. D. Murnaghan, Proc. Natl. Acad. Sci. U.S.A. **30**, 244 (1944).

[24] D. Nguyen Manh, A. Pasturel, A. T. Paxton, and M. van Schilfgaarde, Phys. Rev. B **48**, 14 801 (1993); J. Phys. Condens. Matter **5**, 9087 (1993).

[25] M. J. Kelly and W. M. Stobbs, Phys. Rev. Lett. **45**, 992 (1980).

[26] E. V. Savushkin, V. B. Lapin, and V. E. Egorushkin, J. Phys. Condens. Matter **3**, 9185 (1991).

[27] D. A. Vul and B. N. Harmon, Phys. Rev. B **48**, 6880 (1993).

[28] V. V. Kulagina and M. F. Zhorovkov, Solid State Phys. **1**, 1 (1992).

[29] G. L. Zhao and B. N. Harmon, Phys. Rev. B **48**, 2031 (1993).

[30] G. Bihlmayer, R. Eibler, and A. Neckel, J. Phys. Condens. Matter **5**, 5083 (1993).

[31] J. Xu, W. Lin, and A. J. Freeman, Phys. Rev. B **48**, 4276 (1993).

[32] M. van Schilfgaarde, A. T. Paxton, A. Pasturel, and M. Methfessel, in *Alloy Phase Stability and Design*, edited by G. M. Stocks, D. P. Pope, and A. F. Giamei, MRS Symposia Proceedings No. 186 (Materials Research Society, Pittsburgh, 1991), p. 41.

[33] D. Nguyen Manh, A. T. Paxton, D. G. Pettifor, and A. Pasturel, Intermetallics **3**, 9 (1995).

[34] A. E. Dwight and P. A. Beck, Trans. AIME **215**, 976 (1959).

[35] A. K. Sinha, Trans. AIME **245**, 911 (1969).

[36] A. Zunger, in *Statics and Dynamics of Alloy Phase Transformations*, edited by P. E. A. Turchi and A. Gonis, NATO Advanced Study Institute, Series B: Physics, Vol. 319 (Plenum, New York, 1994), p. 361, and references therein.

[37] Z. W. Lu, S. H. Wei, A. Zunger, S. Frota-Pessoa, and L. G. Ferreira, Phys. Rev. B **44**, 512 (1991).

[38] M. Asta, D. de Fontaine, M. van Schilfgaarde, and M. Methfessel, Phys. Rev. B **46**, 5055 (1992).

[39] Z. W. Lu, S. H. Wei, A. Zunger, and L. G. Ferreira, Solid State Commun. **78**, 583 (1991)

[40] C. Wolverton, G. Ceder, D. de Fontaine, and H. Dreysse, Phys. Rev. B **48**, 726 (1993)

[41] D. H. Le, C. Colinet, P. Hicter, and A. Pasturel, J. Phys. Condens. Matter **3**, 7895 (1991); **3**, 9965 (1991).

[42] C. Colinet and A. Pasturel, Physica B **192**, 238 (1993).

[43] A. Pasturel, C. Colinet, A. T. Paxton, and M. van Schilfgaarde, J. Phys. Condens. Matter **4**, 945 (1992).

[44] C. Colinet *et al.* (unpublished).

[45] J. A. Baker, Proc. R. Soc. London Ser. A **216**, 45 (1953).

[46] R. Kikuchi, J. Chem. Phys. **60**, 1071 (1974).

[47] C. Sigli and J. M. Sanchez, Acta Metall. **33**, 1097 (1985).

[48] R. Kikuchi and J. Murray, Calphad **9**, 311 (1985).

[49] G. Moraitis and F. Gautier, J. Phys. F **7**, 1421 (1977); **7**, 1841 (1977); **8**, 1653 (1978).
[50] M. Sluiter, D. de Fontaine, X. Q. Guo, R. Podloucky, and A. J. Freeman, Phys. Rev. B **42**, 10 460 (1990).
[51] A. J. Dindsdale (unpublished).
[52] A. E. Carlsson, Phys. Rev. B **35**, 4858 (1987).
[53] R. Lück and I. Arpshofen, Thermochim. Acta **131**, 171 (1988).
[54] Yu O. Esin, M. G. Valishev, A. F. Ermakov, O. V. Gel'd, and M. S. Petrushevsku, Russ. J. Phys. Chem. **55**, 421 (1981).
[55] O. Kubaschewski, Trans. Faraday Soc. **54**, 814 (1958).
[56] J. C. Gachon, M. Notin, and J. Hertz, Thermochim. Acta **48**, 155 (1981).
[57] G. D. Garbulsky and G. Ceder, Phys. Rev. B **49**, 6327 (1994).